Magneto-optical imaging and electromagnetic study of $YBa_2Cu_3O_7$ vicinal films of variable thickness

A. Polyanskii,[1,*] R. L. S. Emergo,[2] J. Z. Wu,[2] T. Aytug,[3] D. K. Christen,[3] G. K. Perkins,[4] and D. Larbalestier[1]
[1]*Applied Superconductivity Center, University of Wisconsin-Madison, Wisconsin 53706, USA*
[2]*Department of Physics and Astronomy, University of Kansas, Lawrence, Kansas 66045, USA*
[3]*Oak Ridge National Laboratory, Oak Ridge, Tennessee 37831, USA*
[4]*Blackett Laboratory, Imperial College of Science Technology and Medicine, London, UK*
(Received 8 June 2005; published 15 November 2005)

Magneto-optical imaging (MO) and electromagnetic studies have been applied to measure anisotropy and critical currents (J_c) of $YBa_2Cu_3O_7$ (YBCO) films with variable thickness of 0.2, 0.5, 1.0, 2.0, and 3.0 μm deposited on flat and vicinal $SrTiO_3$ substrates of 10 degree miscut angle (θ_s). The flat films nucleated in island-type mode and developed with a dominant *c*-axis orientation with minority misoriented grains at larger thickness of overall dense structure. The vicinal films, on the other hand, nucleated in step-flow mode and developed with a highly porous structure and minimal density of misoriented grains and impurity phases at large thickness. The difference in the microstructures of these two types of films results in different J_c vs. thickness behaviors. The MO images showed that the magnetic flux penetration in the flat samples is isotropic at all thicknesses, while it is highly anisotropic in the vicinal samples. The anisotropy decreases with film thickness and temperature. These results correlate with distinctive patterns of microstructural evolution in flat and vicinal YBCO films with increasing thickness.

DOI: 10.1103/PhysRevB.72.174509 PACS number(s): 84.71.Mn, 84.30.Jc

I. INTRODUCTION

Coated conductors have been regarded as the second-generation high-temperature superconducting (HTS) wires, in which long lengths of highly grain-oriented HTS coatings are epitaxially deposited on metal tapes.[1,2] This approach is the key to overcoming the problem of "weak-link" current transport across high-angle grain boundaries (GBs) in HTS films[3] and may offer an attractive alternative to the first-generation Bi-HTS powder-in-tube tapes. Coated conductors are expected to carry large currents on the order of a few hundreds to 1000 amperes per centimeter width. Typical critical current density (J_c) of $YBa_2Cu_3O_{7-\delta}$ (YBCO) thin films (regarding thickness typically below 0.3 μm in the rest of this paper), is around 4–5 MA/cm^2 at 77 K and zero applied magnetic field. This means that YBCO films with thickness ranging from a few to several micrometers must have a similar J_c in order to carry the required high current (300 A/cm width for practical applications). Unfortunately, J_c often suffers a dramatic decrease with increasing film thickness in several types of HTS films including YBCO,[4–7] $Tl_2Ba_2CaCu_2O_{8-\delta}$,[8] and $HgBa_2CaCu_2O_{6-\delta}$.[8,9] Some reports show that J_c decreases by a factor of 2–5 when the film thickness increases from $\sim$0.2 to $\sim$1.0 μm. At larger thickness ($>$1.0 μm), J_c continues to decrease but at a much slower pace. Understanding the mechanism of the J_c-thickness (J_c-t) behavior is important for the applications of coated conductors.

It is well established that, even in thin HTS films having optimal superconducting transition temperature (T_c), J_c can still be sensitively affected by film crystallinity and microstructure, such as in-plane and out-of-plane misorientations, and various growth defects. On single-crystal substrates, the misorientations of thin HTS films are typically less than one degree, while on coated conductors this value is 5–10 times larger. It is therefore not surprising that the J_c values are generally higher in HTS films grown on single-crystal substrates, although a comparable J_c has been reported on champion coated conductor samples.[7] With increasing film thickness, the film microstructure evolves under strong influence of the nucleation layer at the film/substrate interface. Island-type spiral growth behavior has been reported for YBCO thin films on nonvicinal (we describe such films as "flat" in the rest of this paper) single-crystal oxide substrates having reasonably small lattice mismatch.[10,11] In this system, depending on the substrate material and processing condition, variation of the film microstructure occurs at large film thicknesses typically in the range of 0.5 to 1.0 μm. Formation of voids and misoriented YBCO grains,[4,6,12] together with significantly degraded J_c, were reported in the upper layer of thick YBCO films. The occurrence of the misoriented grains in thick YBCO films can be avoided if the island-type spiral growth is replaced with step-flow growth in vicinal YBCO films. As shown in our recent study, no misoriented grains were observed in vicinal YBCO films of up to 3.0 μm thickness.[13] Interestingly, while these thick vicinal YBCO films have a highly porous microstructure, they can carry an overall higher J_c than their flat counterparts. This motivated us to carry out a systematic study of the microstructural evolution and its correlation to the J_c behavior in 10° vicinal YBCO films of variable thickness. In this paper, we present our experimental results and discuss the mechanism responsible for the observed J_c behavior.

II. EXPERIMENT

Figure 1 illustrates the orientation of the major crystalline axes of a vicinal substrate and θ_s is the miscut angle defined

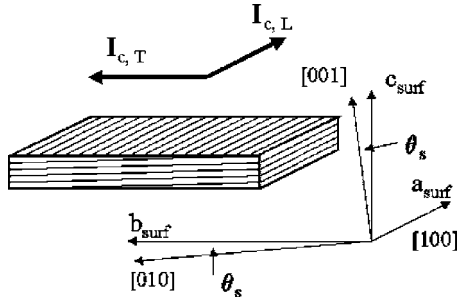

FIG. 1. Schematics of a vicinal film grown on a miscut substrate of tilt angle of θ_s and definition of longitudinal critical current ($I_{c,L}$) and transverse one ($I_{c,T}$). The a_{surf}, b_{surf}, and c_{surf} correspond to the *a*-, *b*-, and *c*-axes, respectively, without the miscut tilting of θ_s.

as the angle between the ⟨001⟩ axis and the normal of the substrate. In this experiment, vicinal $SrTiO_3$ (STO) substrates with $\theta_s = 10°$ along the ⟨010⟩ axis were selected. The substrates were cut into squares of sides of 2.5–5.0 mm, with the ⟨100⟩ axis aligned with a substrate edge. It should be realized that the superconducting critical current (I_c) is anisotropic in the HTS vicinal films. The anisotropy is quantified by the ratio of the longitudinal current $I_{c,L}$ that flows parallel to the steps and the transverse current $I_{c,T}$ that flows perpendicular to the steps. This anisotropy originates from the layered structure of HTS. The reported electronic anisotropy for YBCO is $\gamma = (m_c/m_{ab})^{1/2} = 5-7$, where m_c and m_{ab} are the electron effective masses along the *c*-axis and in the *ab*-plane, respectively. On vicinal YBCO films, the longitudinal current $I_{c,L}$ is *ab*-plane current while the transverse current $I_{c,T}$ has components along both the *ab*-plane and *c*-axis. The anisotropy between $I_{c,L}$ and $I_{c,T}$ in vicinal HTS films is therefore expected to be lower than that between I_c values along the *ab*-plane and *c*-axis, which is consistent with the experimental results reported by many groups on thin HTS vicinal films.[14–19] In addition, improved magnetic flux pinning was reported on thin vicinal HTS films [15,19] due to formation of columnar or planar defects along the normal of the film as resulted from the antiphase grain boundaries that nucleate along the substrate surface steps.[15] Since most previous studies are on thin vicinal films,[14–17] questions remain about how the anisotropy of the I_c evolves with increasing film thickness, and whether improved flux pinning can be obtained in thicker vicinal YBCO films due to the possibility of higher defect density formation. These questions motivated this paper.

Pulsed-laser deposition (PLD) was employed to fabricate YBCO films on flat and 10° vicinal STO substrates. A Lambda Physik KrF excimer laser with $\lambda = 248$ nm and pulse duration of 25 ns was used for deposition. The laser energy density was estimated to be 2–3 J/cm^2. The substrates were silver pasted to the heater and deposition was made at 810 °C in 400 milliTorr oxygen partial pressure. After film deposition, the samples were annealed *in situ* at 520 °C for 45–60 min in 350 Torr of oxygen partial pressure. The deposition rate was about 0.6 Å/pulse at a 5 Hz repetition rate. To ensure a uniform deposition condition for the YBCO films of the same thickness, the flat and vicinal YBCO films were made in the same run by placing the substrates next to each other. For some thicknesses, several sets of flat and vicinal YBCO films were fabricated to confirm run-to-run reproducibility.

The crystalline structure and phase purity of the films were investigated by using x-ray diffraction (XRD), and surface morphology was analyzed using a LEO 1550 field-emission scanning electron microscope (SEM). The superconducting properties of the YBCO films were magnetically characterized in a superconducting quantum interference device magnetometer (Quantum Design) with the external magnetic field (H) applied normal to the film surface. Magnetization (M) versus temperature (T) curves measured on heating in 1.0 mT field after zero-field cooling to 10 K were used to determine the superconducting transition temperature (T_c). M versus H loops were taken at different temperatures between 60 and 85 K for evaluation of the J_c. The Bean model[20] was applied for calculation of the J_c using the overall film dimensions.

To investigate the J_c anisotropy, magneto-optical (MO) characterization was performed using a Bi-doped magneto-optical garnet film with in-plane magnetization grown on gadolinium gallium garnet substrates.[21,22] The sample was mounted on a cold finger of a continuous flow optical cryostat capable of cooling to ~6 K located on an X-Y stage of a polarized optical microscope in reflective mode. A silicone heat sink compound created a tight temperature contact between the bottom face of the sample and the cold finger. To register the normal component of the magnetic flux distribution H_z on the sample surface the indicator film was placed on the top sample face without any restraint. A silicon diode and the LakeShore temperature controller adjusted the sample temperature. The external magnetic field was applied perpendicular to the film plane by a small solenoid surrounding the cold finger.[21,22] A digital camera was used to record the magneto-optical images. We used a deconvolution procedure,[23] as well as the measurements of depth of flux penetration into films,[24,25] to calculate the J_c distribution and its anisotropy in flat and vicinal samples.

III. RESULTS

A. Structure and morphology

All YBCO films grown on flat STO substrates have a *c*-axis orientation as determined from the XRD θ-2θ curves. At small thickness $\leqslant 0.5$ μm, no other peaks were visible, suggesting only *c*-axis growth in this thickness range. In addition, no other impurity phases were visible from the XRD spectra in this thickness range. With increasing film thickness >0.5 μm, the YBCO (200) peak appears, indicating the formation of *a*-axis-oriented grains in thicker YBCO films on flat STO substrates. This observation is consistent with the previous reports.[6] In addition, small volume portions of misoriented phases including (111) and (112) were also observed. To quantify the out-of-plane texture evolution, (005) rocking curves (ω-scan) were taken on five flat samples of 0.2, 0.5, 1.0, 2.0, and 3.0 μm thickness, respectively. The full width at half-maximum (FWHM) of the (005) ω-scan of flat YBCO films (open triangles) is shown as function of thickness in Fig. 2. At the 0.2 μm film thickness, the FWHM

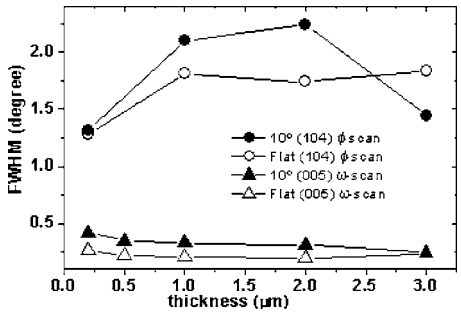

FIG. 2. The FWHM values of XRD (104) φ-scans (circles), and (005) ω-scales (triangles) measured on flat (open symbols) and 10° vicinal (solid symbols) YBCO films with thickness in the range of 0.2 to 3.0 μm.

has the maximum value of 0.26°, and experienced a monotonic decrease with increasing thickness to the minimum value of 0.19° at 2.0 μm film thickness, followed by an upturn to 0.24° at 3.0 μm. This more-or-less constant FWHM value in the thickness range of 0.5 to 3.0 μm suggests that the degradation of the microstructural degradation in flat YBCO films manifests mostly in the form of misoriented grains, which have large-angle GBs with the c-axis-oriented YBCO matrix and obstruct I_c.

When the miscut substrates are employed, the c-axis of YBCO is supposedly tilted (see Fig. 1) at a small miscut angle θ_s with respect to the normal of the film. To confirm this, XRD pole figures and θ-2θ scans were taken on vicinal samples of different thickness. Neither impurity nor misoriented YBCO phase was observed. The tilt angle of around 10°–11° was observed between the c-axis and the normal of the film for these samples. The observation of four (104) poles that are 90° apart confirmed epitaxy of YBCO films on the miscut substrates.

The FWHM values of the (005) pole for the vicinal YBCO films are also included in Fig. 2 (solid triangles). Qualitatively, a similar monotonic decrease of the FWHM with increasing thickness was observed, while quantitatively, the (005) FWHM values are slightly higher in the vicinal YBCO films than that of the flat ones at the same thickness. For example, the FWHM is 0.43° at 0.2 μm thickness and decreased to 0.31° at 2.0 μm thickness. This is not unexpected because of the large strain induced in vicinal YBCO films when the lattice is slightly tilted with respect to the substrate normal. At larger thickness of 3.0 μm, the FWHM continue to decrease to about 0.25°, which is comparable to that of flat YBCO films of the same thickness. This means that the out-of-plane grain alignment continues to improve with increasing thickness up to 3.0 μm. If this trend continues beyond 3.0 μm thickness, better out-of-plane grain alignment can be obtained in vicinal YBCO films.

The in-plane texture evolution as function of thickness was characterized using (104) ϕ-scans. The FWHM of the (104) peak is shown as function of film thickness for both flat (open circles) and vicinal (solid circles) samples in Fig. 2. Overall, the in-plane FWHM value is higher than the out-of-plane one by a factor of 2–10. On flat samples, the (104) FWHM value increased from ~1.2° at 0.2 μm thickness to 1.7° at 1.0 μm thickness and remained approximately a constant at larger thickness. The (104) FWHM on the vicinal samples took a similar trend, despite a slightly higher value, in smaller thickness up to 2.0 μm thickness, which was followed by a drop at 3.0 μm thickness. In fact, smaller out-of-plane misorientation was observed in vicinal YBCO film at this thickness. This difference may be attributed to the different patterns in nucleation that occurred in the flat and vicinal YBCO films. As we mentioned earlier, the flat YBCO film nucleates via a spiral island-type mode while the vicinal film, step-flow mode. It is not a surprise that microstructure evolves in different patterns in these two types of films.

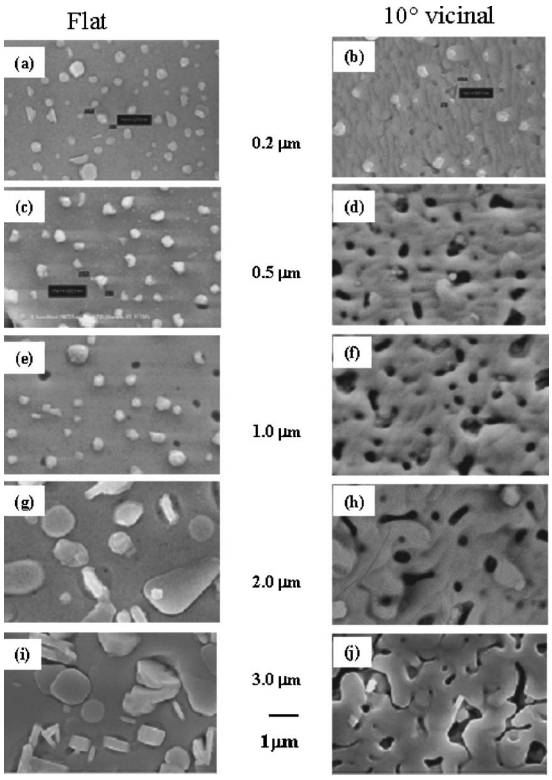

FIG. 3. SEM pictures of YBCO films deposited on flat (left column) and 10° miscut (right column) STO substrates. The rows show the progression (from top to bottom) with respect to film thickness. Top row: 0.2 μm thick YBCO films on (a) flat and (b) 10° miscut STO. Second row: 0.5 μm thick YBCO films on (c) flat and (d) 10° miscut STO. Third row: 1.0 μm thick YBCO films on (e) flat and (f) 10° miscut STO. Fourth row: 2.0 μm thick YBCO films on (g) flat and (h) 10° miscut STO. Fifth row: 3.0 μm thick YBCO films on (i) flat and (j) 10° miscut STO.

To understand how microstructure evolved in the flat and vicinal YBCO films, the film surface morphology was analyzed using SEM. Figure 3 shows two sets of SEM micrographs taken on YBCO films of 0.2, 0.5, 1.0, 2.0, and 3.0 μm thickness on flat (left column) and 10° miscut (right column) STO substrates, respectively. It is clearly seen that the two YBCO film sets experienced dramatically different characteristics of microstructural evolution. On flat STO, all films look dense, despite an increasingly rougher surface morphology at larger film thickness.

Two factors contributed to the surface roughness of the flat YBCO films at large thickness. The first one is the particulate, typical of the PLD YBCO films, the dimension of

which increased from sub-micrometer to ~1.0 μm when the film thickness was increased from 0.2 to 3.0 μm. The other is the misoriented YBCO phases shown as rectangular bars (actually they are sides of plates) and other shaped features on the surface of the flat YBCO films when the film thickness is near or above 1.0 μm. This is consistent with the appearance of the misoriented phases in the flat YBCO films with thickness >0.5 μm in XRD analysis. The density and volume fraction of these misoriented phases increase with film thickness. In the case of miscut substrates, the YBCO films followed step-flow growth characteristics, as evidenced by the observed atomic steps on films with thicknesses up to 2.0 μm in the right column of Fig. 3. Particulates with a much lower density can also be seen at 0.2 μm thickness but they are barely observable at larger thickness, in sharp contrast to the flat YBCO film case.

In addition, no misoriented grains were visible on the surface of the vicinal films, consistent with the XRD data discussed earlier. A distinctive difference between the flat and vicinal YBCO films is that the latter are highly porous when the thickness is $\geqslant$0.5 μm. Even at 0.2 μm thickness, pores of a circular shape are already visible with dimension of tens to hundreds of nanometer. With increasing thickness, both the shape and density of the pores vary. Starting from ~0.5 μm thickness, circular and rectangular shaped (or dog-bone shaped) pores become a distinctive feature. The sides of most rectangular pores are either perpendicular or parallel to the steps, suggesting that the strain built through vicinal film may contribute dominantly to the formation of the pores. Some of the rectangle pores connected to form a straight angle pore. Nevertheless, steps are still visible on most parts of the film, while the step width increased by 50%–100% from 0.2 to 2.0 μm thickness. When the film thickness is further increased, a melted-cheese type of surface morphology was observed on the vicinal YBCO films [see Fig. 3(j)]. Large irregular shaped pores were visible all over the film, while steps disappeared nearly completely.

The appearance of pores in vicinal YBCO films may directly relate to the strain induced in the tilt YBCO crystal lattice. This strain may cause distortion, resulting in higher in-plane and out-of-plane misorientations as suggested in the XRD analysis (Fig. 2). Although the exact mechanism for the pore formation is still under investigation, we speculate that the release of the local strain on the lattice is the major reason. The strain seems reduced significantly at large thickness above 2.0 μm so that both the in-plane and out-of-plane misorientations reduced accordingly. Interestingly, this was accompanied with disappearance of the J_c anisotropy, as we will discuss later in the MO imaging (MOI) study.

B. Magnetic characterization of T_c and J_c

The zero-field-cooled (ZFC) M-T curves were measured on both sets of YBCO films to determine their T_c. The YBCO films on both flat and miscut substrates showed uniform superconducting transitions even though the film thickness was varied by an order of magnitude. The T_c values for both flat and vicinal YBCO samples are in the range of 87.8–88.5 K. These slightly lower T_c values than the ones typically reported for YBCO films were due to an offset of ~−1.0 K in the temperature sensor of our magnetometer. The observed uniformity in T_c suggests that the variation in the processing condition for YBCO films was insignificant with increasing film thickness.

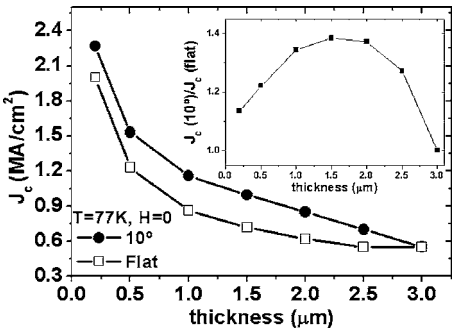

FIG. 4. J_c-thickness curves for YBCO films deposited on flat (open squares) and 10° miscut (solid circles) STO substrates at 77 K and SF. The relative enhancement of the J_c in 10° vicinal YBCO films, defined as J_c (10°)/J_c (flat), is plotted in the inset as function of film thickness.

The J_c values were calculated from the Bean model[20] using the dimensions of the films. Figure 4 compares the thickness dependence of J_c at 77 K and self-field for flat and vicinal YBCO films. It should be mentioned that the J_c-thickness behavior of YBCO on flat STO agrees well with what other groups have reported.[4,6,7] In the thickness range investigated, both film sets showed a similar trend of monotonic decrease of J_c with increasing film thickness. However, the vicinal YBCO films carry higher J_c values than the flat ones in the entire thickness range. It should be realized that J_c is anisotropic in vicinal YBCO films,[14–19] and the magnetically measured J_c values shown in Fig. 4 represent a value closer to the lower transverse J_c component ($J_{c,T}$) of the current loop in the vicinal films.[26]

The anisotropy of J_c has been confirmed both by MOI studies as discussed later in this paper and by transport measurements. In a parallel study of the transport J_c of YBCO films made on 15° miscut STO substrates using the same processing conditions reported here,[13] two bridges were patterned, with one along the longitudinal and the other along the transverse direction. The transverse transport $J_{c,T}$ was confirmed to be consistent with the magnetic J_c measured on the same sample before lithography, while the longitudinal transport J_c was much higher. This means that that much higher J_c values along the longitudinal direction are expected on vicinal YBCO films. The inset of Fig. 4 depicts the relative improvement of J_c in 10° vicinal YBCO films as opposed to their flat counterparts at different thickness. Starting from ~16% improvement at 0.2 μm, the J_c improvement reached the maximum of ~46% at 1.0 μm thickness, followed by monotonic decrease to ~28% at 2.5 μm thickness. At 3.0 μm thickness, the vicinal and flat YBCO films have nearly the same J_c.

C. Magneto-optical imaging

A set of flat and 10° vicinal YBCO films with thickness of 0.2, 0.5, 1.0, 2.0, and 3.0 μm have been used for MO imag-

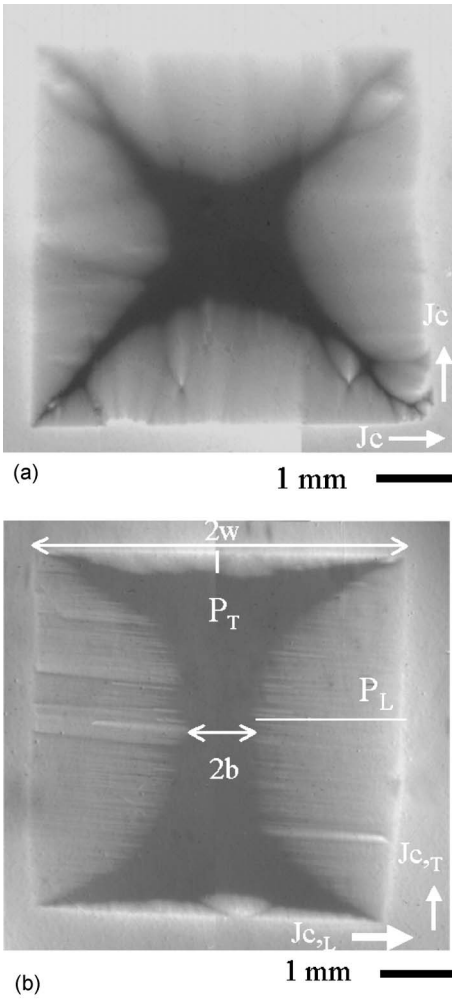

FIG. 5. MO images of flux behavior in the 0.2 μm thick flat (a) and 10° miscut (b) YBCO samples taken at temperatures $T=10$ K. $2w$ is the sample width, $2b$ is the width of flux-free Meissner region and P_L and P_T are the depths of flux penetration perpendicular and parallel to the steps of growth, respectively. ZFC regime has been used at $T=10$ K and (a) $H=80$ mT and (b) $H=28$ mT. The symmetric roof patterns of flux penetration with well-developed diagonal d-lines, where current change direction on 90°, are well visible in dark contrast.

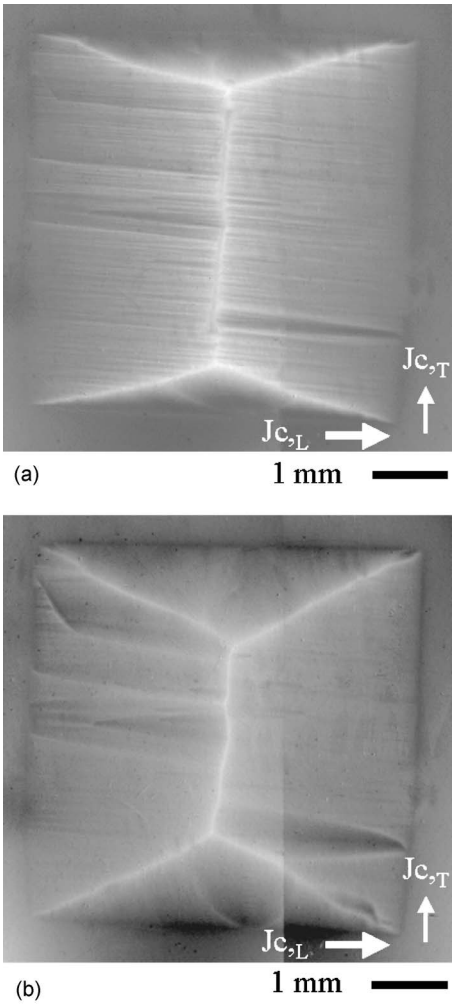

FIG. 6. MO images of flux behavior in the 0.2 μm thick 10° vicinal YBCO samples taken at temperatures (a) 10 K and (b) 60 K. Remnant state was obtained after cooling down in $H=120$ mT. Additional to the symmetric roof patterns visible in bright contrast the filamentary picture of flux penetration exists at $T=10$ K (a).

ing at temperature range 10–80 K and H fields as high as 120 mT. Anisotropy of the J_c was confirmed on 10° vicinal films. Figures 5 and 6 present the MO images taken at $T=10$ and 60 K, respectively, on a flat and a 10° vicinal YBCO film with the thickness of 0.2 μm. The flat sample [Fig. 5(a)] has quite uniform superconducting properties everywhere around the sample. In homogeneous superconductors of square or rectangular shapes, magnetic flux starts penetrating at the middle of the sample edges[25] and forms a "roof" pattern with well-developed diagonal lines (discontinuity d-line). These lines are well visible on MO image in Fig. 5(a) in dark color contrast when H field was increased to 80 mT. The flux carrying regions have the bright contrast. The dark square at the center of the sample expels the external magnetic field and only the Meissner current circulates in this area. The behavior of magnetic flux in the flat sample is well described by the Bean model.

In contrast to the flat samples, the 10° vicinal YBCO sample showed in the ZFC regime a very anisotropic flux penetration along and perpendicular to the steps of growth on miscut substrate at $H=28$ mT [Fig. 5(b)]. The magnetic flux penetrates more easily along the P_L direction due to the anisotropic pinning force of parallel oriented planar antiphase boundaries[15,26] generated in vicinal films during epitaxial growth and exhibits a specific filamentary pattern. These defects are strong pinning centers transverse to the boundaries, and the $J_{c,T}$ is smaller than the J_c in the flat film. It is clearly seen in Fig. 5(b) that the magnetic flux penetrates into the sample along P_L direction deeper than in the flat sample, even at lower field $H=28$ mT.

Figures 6(a) and 6(b) show magnetic flux behavior in the 10° vicinal sample in remnant state at 10 and 60 K, respectively, when the external field was reduced from 120 mT to zero. The filamentary pattern on MO image is more remarkable at the lower temperature in the remnant state. The fila-

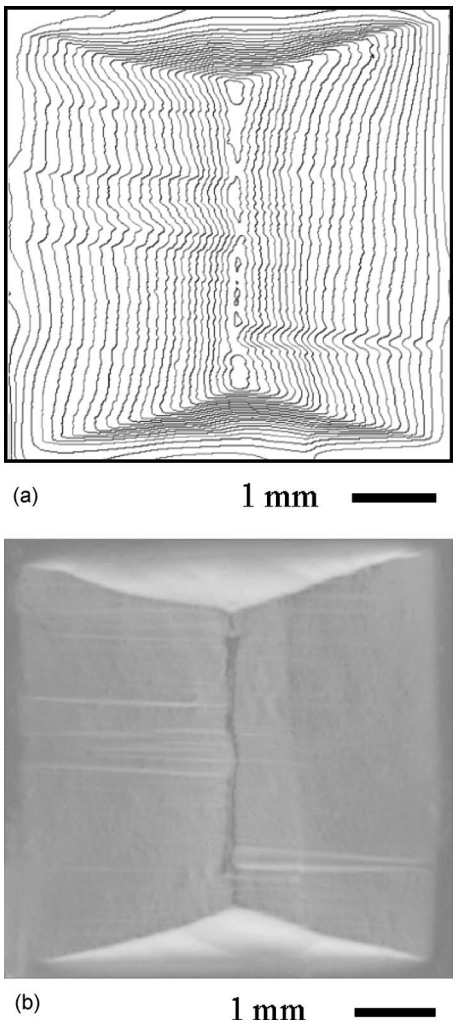

FIG. 7. (a) Contours of the magnetization current streamlines and (b) current distribution map calculated by deconvolution procedure for MO image of the same sample in Fig. 6(a) in remnant state. The diagonal *d*-lines exist where current turns on 90°.

mentary flux pattern and a few macroscopic sphenoid defects are also better seen than in the ZFC state in Fig. 5(b). This filamentary flux pattern has also been observed early and connected with variations in the structural width of parallel oriented planar antiphase boundaries.[27,28] With increasing temperature to 60 K and higher, the MO images showed that the anisotropy of flux penetration is slowly decreasing and the apex angle is changing from 150° at $T=10$ K to 125° at $T=60$ K and further to 118° at $T=77$ K. At $T=60$ K the filamentary pattern and sphenoid defects are hardly visible.

Figures 7(a) and 7(b) show the streamlines and map of magnetization current extracted by deconvolution procedure.[23] The calculated images confirmed a very anisotropic current distribution in the vicinal film. The streamlines are much more dense in the direction of the growth steps and consequently the $J_{c,L}$ is much larger than $J_{c,T}$. As seen in Fig. 7(a), the streamlines of the magnetization current flow uniformly along all edges of sample and change direction on 90° directly on the *d*-lines where the strong contrast appears on magneto-optical images.

The map of current distribution shows different intensity contrasts, which reflect the values of I_c flowing parallel and perpendicular to growth steps. The segments on the top and bottom of the image are brighter than in the direction perpendicular to steps of growth. The intensity of the contrast ratio reflects the anisotropy of the critical current. The $J_{c,L}$ is about 3.5 times higher than the $J_{c,T}$ and this ratio is in good agreement with the anisotropy of critical currents taken by MO on a similar YBCO sample (0.24 μm thick 10° vicinal film) at 4.2 K.[29]

In contrast to the vicinal sample the streamlines and map of magnetization current extracted by deconvolution procedure in the flat sample show uniform value of the current distribution around the sample. The uniform flux penetration in the flat sample does not change very much with increasing temperature to 77 K and the apex angle of 90° between diagonals remained the same at a wide temperature range. Only at $T=80$ K have we observed that the shape of the roof pattern has slightl nonuniformity of current distribution.

To study the temperature and field dependences of the critical current on flat and 10° vicinal samples with different thickness, the lengths of the flux penetration P from edges of flat and 10° vicinal YBCO samples, as well the $2b$ width, were measured [see Fig. 5(b)]. We were able to extract the anisotropy, absolute value, and temperature dependence of J_c in ZFC and FC regimes using the procedure well described in Refs. 24 and 25. The procedure is based on the Eq. (3) in Ref. 25: $b(B_a)=w/\cosh(B_a/B_0)$. Here, $2b$ is the width of a vortex-free region, the so-called Meissner area, $2w$ is the width of sample in the direction of flux penetration [see Fig. 5(b)], B_a is the external magnetic field, and $B_0=\mu_0 J_c d/\pi$ is the characteristic field of full flux penetration.[24,25] By inverting Eq. (3) under the assumption that there is no field dependence of J_c in the low magnetic field range less than 120 mT, the expression for calculation of J_c is given by $J_c=\pi B_a/d\mu_0 a\cosh[w/b(B_a)]$, where d is the thickness of the YBCO film. To obtain the T-dependence of J_c, we have measured $2b$ at several T and H values. We have found that the J_c does not depend on H in T range of 8–80 K, when H is less than the field of full flux penetration B_0. At low T, the B_0 is 120 mT. The same observations were made at T around 77–80 K, where the maximum H of 10–20 mT was less than B_0. We have plotted B_a versus $a\cosh[w/b(B_a)]$ and found that the equation $\pi B_a=J_c d\mu_0 a\cosh[w/b(B_a)]$ has a constant slope at each T. As seen from this equation, each slope is proportional to the critical current J_c at the given T. The same results have been found in thin YBCO films in our earlier paper (see insets in Figs. 15 and 16 in Ref. 25).

Figure 8 presents the T dependence of J_c in the 0.2 μm thick flat and 10° vicinal YBCO samples calculated according to the above-described procedure using MO images taken in T range of 10–80 K. As seen from the plot, the $J_{c,L}$ (closed triangles) is much higher than the $J_{c,T}$ (closed squares), but in the flat sample (closed circles) the J_c has values even higher than $J_{c,L}$ at low temperatures $\leqslant 15$ K. However with increasing temperature the J_c of the flat sample decreases faster and becomes lower than $J_{c,L}$ and even lower than $J_{c,T}$ at $T\geqslant 50$ K. The plot of the anisotropy of J_c in the 10° vicinal YBCO sample with 0.2 μm thicknesses is shown as a function of T in the inset of Fig. 8. The

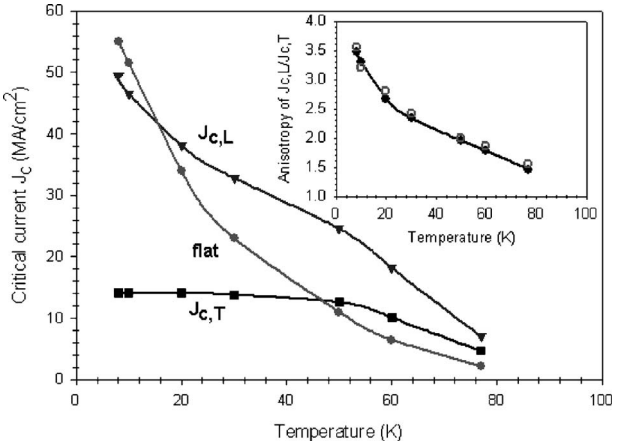

FIG. 8. T dependence of J_c in the 0.2 μm thick flat and 10° vicinal YBCO samples. $J_{c,L}$ and $J_{c,T}$ are critical currents directions perpendicular and parallel to steps of growth in vicinal YBCO sample, respectively. Inset: T dependence of the J_c anisotropy ($J_{c,L}/J_{c,T}$) in the vicinal sample calculated in ZFC (solid) and FC (open) modes.

solid circles are the MO experimental data in the ZFC regime, and the open circles, are the calculated ratio of P_L/P_T in remnant mode. Both measurements show the same results, namely, the influence of the growth steps is slowly disappearing with increasing temperature. Similar behaviors of J_c-T and J_c anisotropy versus T were also observed on the 0.5 μm thick flat and 10° vicinal YBCO samples where only the absolute values of the J_c for both samples were less than in 0.2 μm thick ones.

In the samples with thickness $\geqslant$2.0 μm the J_c in the flat sample is higher than $J_{c,L}$ and $J_{c,T}$ in the vicinal sample in the whole T range of 10–77 K. Figures 9 and 10 show, respectively, the data taken on the 2.0 and 3.0 μm thick samples (symbols are the same as in Fig. 8). The $J_{c,L}$ and $J_{c,T}$ in the 2.0 μm thick vicinal YBCO sample are still different, but both are lower than the J_c in the flat sample (Fig. 9). The anisotropy (the inset of Fig. 9) has the same tendency with

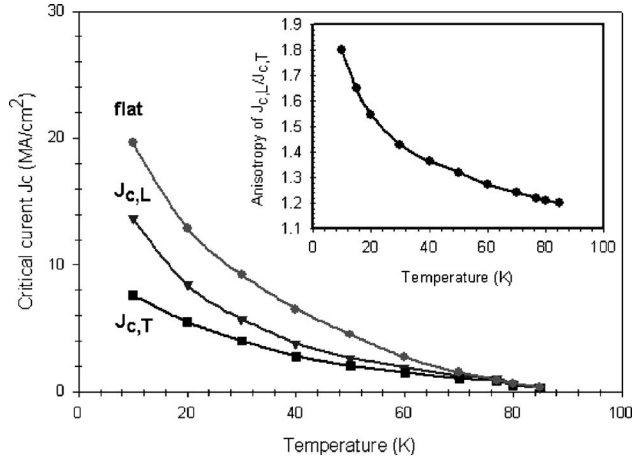

FIG. 9. T dependence of J_c in the 2.0 μm thick flat and 10° vicinal YBCO samples. Inset: T dependence of the J_c anisotropy ($J_{c,L}/J_{c,T}$) in this vicinal sample. The anisotropy of J_c was calculated in ZFC.

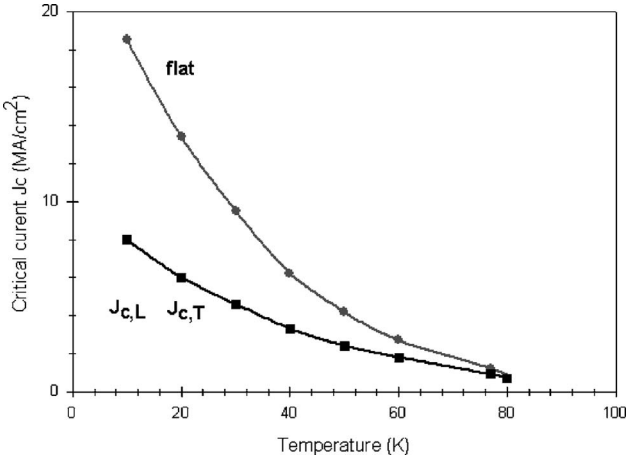

FIG. 10. T dependence of J_c in the 3.0 μm thick flat and 10° vicinal YBCO films. The 3.0 μm thick 10° vicinal sample does not show any remarkable anisotropy, and $J_{c,L}$=$J_{c,T}$.

absolute value less than that in thinner samples. At the 3.0 μm thickness, the J_c anisotropy diminishes completely in the vicinal sample (Fig. 10). The MO images in Figs. 11(a) and 11(b) taken on the 10° vicinal film with 3.0 μm thickness demonstrate no influence of steps of growth at T =10 K and 77 K, respectively. The apex angles between diagonal d-lines of the roof pattern in both images are 90°.

The decreasing J_c anisotropy with increasing thickness at a fixed T was observed in the vicinal films. The same tendency, as mentioned before, was also observed at fixed thickness when temperature was increased from 10 to 77 K. Figures 12(a) and 12(b) summarize the thickness dependence of J_c and anisotropy of the flux penetration in flat and 10° vicinal YBCO films at fixed temperatures of 10 K [Fig. 12(a)] and 77 K [Fig. 12(b)], respectively. The J_c values in flat samples and in both directions of the 10° vicinal YBCO samples decrease with increasing thickness. In addition, the J_c anisotropy in the vicinal films also decreases slowly with thickness in the temperature range studied. In the 3.0 μm thick vicinal films there is no remarkable anisotropy in the temperature range from 10 to 77 K.

The flux behavior on MO images in flat films shows that all flat samples with different thickness show quite uniform flux penetration even at T=77 K. The apex angles between the diagonals of the roof pattern are equal to 90° for all flat samples. This means that the J_cs in both directions are the same and that there is no anisotropy of flux penetration in flat samples.

IV. DISCUSSION AND CONCLUSION

In this study, it has been clearly shown (Fig. 12) that the J_c anisotropy decreases monotonically with increasing film thickness on the 10° vicinal YBCO films in the temperature range of 10–77 K. An interesting feature observed in this experiment is the correlation between the J_c anisotropy and J_c values in vicinal samples. Above a certain temperature that is thickness dependent, the J_c values in vicinal films are higher than those of their flat counterparts. For example, the

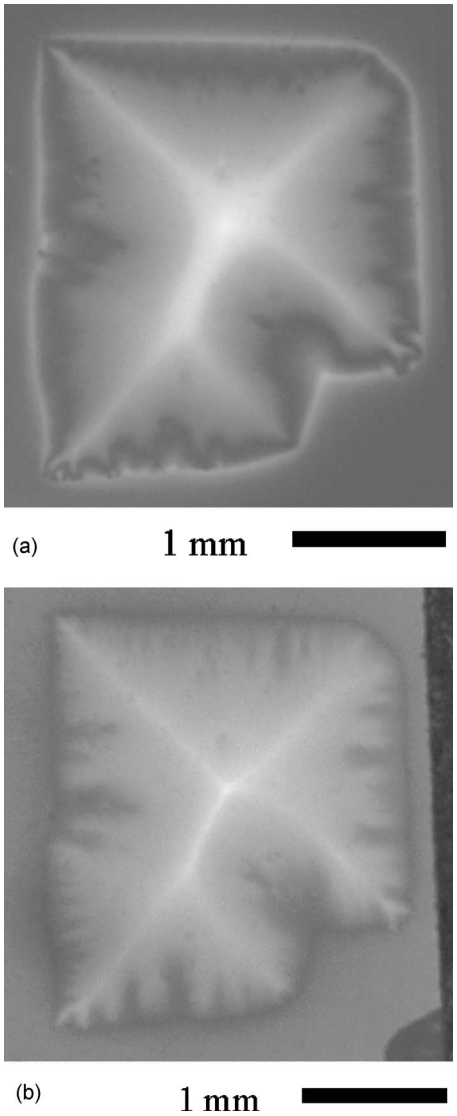

FIG. 11. MO images of flux behavior in the 3.0 μm thick 10° vicinal YBCO samples taken at (a) $T=10$ K and (b) $T=77$ K. Remnant state was obtained after cooling down in $H=120$ mT.

J_c values in the 0.2 μm flat sample (Fig. 8) at temperatures $\leqslant 15$ K are higher than $J_{c,L}$ in 10° vicinal sample, but decrease faster with temperature than $J_{c,L}$. At $T \geqslant 15$ K, a crossover occurred and $J_{c,L}$ became higher. In fact, a second crossover with $J_{c,T}$ followed at $T \sim 45$ K, leading to both $J_{c,L}$ and $J_{c,T}$ being higher than the J_c in the flat film above 45 K. It should be realized that distinct growth steps are present when J_c anisotropy is high. The presence of growth steps may increase the pinning force on magnetic vortices by forcing the vortices to move more preferably perpendicular to the steps because of a much larger current $J_{c,L}$ flowing parallel to the steps. However, in films thicker than 0.2 μm, the influence of growth steps gradually decreases due to the healing of oriented planar antiphase boundaries formed during epitaxial film growth. The J_c anisotropy shown in the inset of Figs. 12(a) and 12(b) slowly decreases with film thickness, and the $J_{c,L}$ and $J_{c,T}$ become comparable in the thickest samples.

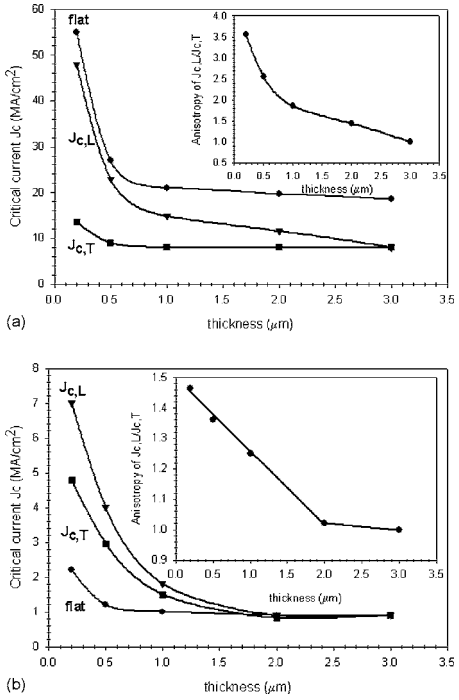

FIG. 12. Thickness dependence of J_cs in flat and 10° vicinal YBCO samples taken at $T=10$ K (a) and $T=77$ K (b). Inset: Thickness dependence of the J_c anisotropy ($J_{c,L}/J_{c,T}$) in vicinal YBCO samples.

However, as shown in the inset of Fig. 12(b), the decrease of J_c anisotropy in vicinal films at $T=77$ K is not as uniform as it is at $T=10$ K. In the former case, the decrease of the J_c anisotropy is linear at a rate of about $-0.22/\mu$m-thickness for sample thickness up to 2.0 μm. With increasing thickness, this decrease slowed down, and at 3.0 μm thickness no J_c anisotropy was observable. The J_c values in flat samples at $T=77$ K are less the $J_{c,T}$ in the vicinal samples in the thickness range between 0.2 and 2.0 μm. Above this thickness, J_c in flat samples is comparable to $J_{c,L}$ and $J_{c,T}$ in the vicinal film.

The decrease of the J_c anisotropy with thickness correlates with the evolution of the film microstructure in vicinal YBCO films as confirmed in SEM (Fig. 3), where the growth steps diminish gradually with thickness while more pores appear. In the thin film regime, the growth steps are clearly seen and the J_c anisotropy is a maximum at all temperatures. The appearance of pores starting at ~ 0.5 μm thickness may be a major factor complicating the microstructural evolution. The thicker vicinal films are highly porous, while the growth steps are hardly visible and are of much larger width. One may speculate that the current in this spongelike matter no longer takes a well-defined path along the specified direction microscopically, resulting in reduced J_c anisotropy. At the maximum thickness of 3.0 μm, the vicinal film looks like a melted cheese. The healing of the steps is accompanied by the diminishing of the J_c anisotropy.

Another distinct feature of the vicinal YBCO films is the disappearance of the misoriented grains, which are typically seen on thick flat YBCO films. The increasing volume portion of misoriented grains is believed to be the major current

obstacle in flat YBCO films of thickness above ~1.0 μm. Indeed, significantly improved J_cs have been demonstrated by refurbishing the growth surface via thin CeO_2 layers after every micrometer of YBCO thickness.[30] Our results indicate that vicinal growth may provide an alternative solution for the misoriented-grain problem in thick YBCO films. This, however, cannot account for the enhanced J_cs in thinner vicinal films.

At 77 K, we have a possibility to compare the J_cs measured by both magnetization and MO methods in the flat and vicinal samples. Since the vicinal samples still have remarkable anisotropy at this temperature, the magnetically measured J_cs is limited by the lower $J_{c,T}$ across the growth steps. However, the magnetization $J_{c,T}$ shows higher values overall in 10° vicinal YBCO films at 77 K and self-field as compared to their flat counterparts of the same thickness (see Fig. 4). These results correlate well with the $J_{c,T}$ taken on vicinal YBCO thin films using MO technique. As seen in Fig. 12(b), the MO-defined $J_{c,T}$ is higher than the J_c in flat films, and agrees qualitatively with the magnetic data in the thickness range less than 2.0 μm. Nevertheless, there is an approximately 2.5 time difference between the MO $J_{c,T}$ and magnetic $J_{c,T}$ at a thickness of 0.2 μm. This discrepancy may be attributed to the difference in defining J_c values in these two techniques. The magnetic J_c represents an average J_c over the entire sample since the calculation was based on the whole film dimension.[20] However any additional gross defects can reduce the measured magnetic moment and consequently reduce the magnetic J_c from the intrinsic value. These irregular defects, as also visible in MO image in Figs. 5(b) and 6(a), can reduce the magnetic $J_{c,T}$ to values lower than that due to planar antiphase boundaries.

In contrast, the magnetic (Fig. 4) and MO [Fig. 12(b)] J_c values in the flat samples are very close at thickness less than 2.0 μm. On the other hand, all flat samples at 77 K exhibit more uniform flux behavior with less remarkable macroscopic defects inside the samples. Some defects are located only along the sample edges, as seen in Fig. 5(a). These defects can also possibly reduce the magnetic J_c, while they practically have no influence on the macroscopic flux front penetration used for definition of the MO J_c values.

In summary, we have fabricated flat and 10° vicinal YBCO films with variable thickness of 0.2, 0.5, 1.0, 2.0, and 3.0 μm. The different YBCO nucleation mechanisms on flat and vicinal substrates resulted in different patterns of microstructural evolution with increasing thickness, and therefore different J_c versus thickness behaviors. The flat films nucleate via island-type mode and develop into *c*-axis-oriented dominant, plus a certain portion of misoriented grains at larger thickness with overall dense structure. The vicinal films, on the other hand, nucleate via step-flow mode and develop into a highly porous structure, with a minimal amount of misoriented grains and impurity phases at large thickness. The vicinal films showed overall higher J_c values at 77 K than their flat counterparts, confirming the correlation between the microstructure and the J_c-thickness behavior. The MO images showed that the magnetic flux penetration in the flat samples is isotropic at different thickness, while it is highly anisotropic in the vicinal samples. The anisotropy decreases with film thickness and temperature. We propose that the interplay between the anisotropic current flow and the porous structure in vicinal YBCO films defined a more favorable current flow path. In coated conductor applications, if the steps are parallel to the tape length, a higher J_c can be obtained by growing YBCO films at a small vicinal angle.

ACKNOWLEDGMENT

J.Z.W. acknowledges supports from NSF for this work. R.E. was supported by AFOSR. The research at ORNL was sponsored by the U.S. Department of Energy under Contract No. DE-AC05-00OR22725 with the Oak Ridge National Laboratory, managed by UT-Battelle, LLC. The work at UW Madison has been supported by MURI DOD-AFOSR, NSF-MRSEC, and DOE-EERE programs.

*Corresponding author, e-mail address: polyansk@engr.wisc.edu

[1] D. K. Finnemore, K. E. Gray, M. P. Maley, D. O. Welch, D. K. Christen, and D. M. Kroeger, Physica C **320**, 1 (1999).

[2] M. Paranthaman, A. Goyal, R. Feenstra, T. Izumi, and V. Selvamanickam, Summary of the 2002 MRS Workshop on Processing and Applications of Superconductors, Gatlinburg, TN, 31 July–2 Aug, 2002.

[3] D. Dimos, P. Chaudhari, and J. Mannhart, Phys. Rev. B **41**, 4038 (1990).

[4] S. R. Foltyn, Q. X. Jia, P. N. Arendt, L. Kinder, Y. Fan, and J. F. Smith, Appl. Phys. Lett. **75**, 3692 (1999).

[5] M. Paranthaman, C. Park, X. Cui, A. Goyal, D. F. Lee, P. M. Martin, D. T. Verebelyi, D. P. Norton, D. K. Christen, and D. M. Kroeger, J. Mater. Res. **15**, 2647 (2000).

[6] B. W. Kang, A. Goyal, D. R. Lee, J. E. Mathis, E. D. Specht, P. M. Martin, D. M. Kroeger, M. Paranthaman, and S. Sathyamurthy, J. Mater. Res. **17**, 1750 (2002).

[7] S. R. Foltyn, P. N. Arendt, Q. X. Jia, H. Wang, J. L. Macmanus-Driscoll, S. Kreiskott, R. F. De Paula, L. Stan, J. R. Groves, and P. C. Dowden, Appl. Phys. Lett. **82**, 25 (2003).

[8] Z. W. Xing, Y. Y. Xie, and J. Z. Wu, Physica C **402**, 45 (2004).

[9] X. Wang, R. Emergo, and J. Z. Wu (unpublished).

[10] L. Luo, M. E. Hawley, C. J. Maggiore, R. C. Dye, and R. E. Muenchausen, Science **251**, 1587 (1991).

[11] C. Gerber, D. Anselmetti, J. G. Bednorz, J. Mannhart, and D. G. Schlom, Nature (London) **350**, 279 (1991).

[12] K. J. Leonard, S. Kang, A. Goyal, K. A. Yarborough, and D. M. Kroeger, J. Mater. Res. **18**, 1723 (2003).

[13] R. L. S. Emergo, J. Z. Wu, D. K. Christen, and T. Aytug, Appl. Phys. Lett. **85**, 618 (2004).

[14] J. Brotz, H. Fuess, T. Haage, J. Zegenhagen, Ch. Jooss, A. Forkl, and R. Warthmann, J. Appl. Phys. **85**, 635 (1999).

[15] Ch. Jooss, R. Warthmann, and H. Kronmüller, Phys. Rev. Lett. **82**, 632 (1999).

[16] L. Mechin, P. Berghuis, and J. E. Evetts, Physica C **302**, 102 (1998).
[17] T. Haage, J. Zegenhagen, J. Q. Li, H.-U. Habermeier, M. Cardona, Ch. Jooss, R. Warthmann, A. Forkl, and H. Kronmüller, Phys. Rev. B **56**, 8404 (1997).
[18] D. H. Lowndes, D. K. Christen, C. E. Klabunde, Z. L. Wang, D. M. Kroeger, J. D. Budai, Shen Zhu, and D. P. Norton, Phys. Rev. Lett. **74**, 2355 (1995).
[19] Y. Y. Xie, J. Z. Wu, S. H. Yun, R. Emergo, and R. Aga, Appl. Phys. Lett. **85**, 70 (2004).
[20] C. P. Bean, Rev. Mod. Phys. **36**, 31 (1964).
[21] A. A. Polyanskii, X. Y. Cai, D. M. Feldmann, D. C. Larbalestier, *Nano-crystalline and Thin Film Magnetic Oxides*, edited by I. Nedkov and M. Ausloos, NATO Science Series 3: High Technology (Kluwer Academic, Dordrecht, 1999), pp. 353–370.
[22] A. A. Polyanskii, D. M. Feldmann, and D. C. Larbalestier, *Magneto-Optical Characterization Techniques*, edited by D. Cardwell, Handbook of Superconducting Materials, University of Cambridge, UK; D. Ginley, NREL (IOP, Bristol, 2003), p. 1551–1567.
[23] G. K. Perkins, Yu. V. Bugoslavsky, and A. D. Caplin, Supercond. Sci. Technol. **15**, 1140 (2002).
[24] E. H. Brandt and M. Indenbom, Phys. Rev. B **48**(12), 893 (1993).
[25] A. A. Polyanskii, A. Gurevich, A. E. Pashitski, N. F. Heinig, R. D. Redwing, J. E. Nordman, and D. C. Larbalestier, Phys. Rev. B **53**(13), 8687 (1996).
[26] For a thin-film sample of square dimensions $a \times a$ with anisotropic $J_{c,L} < J_{c,T}$, the apparent critical current density ($J_{c,app}$) obtained by application of the standard Bean model to the measured magnetization hysteresis (ΔM) is given by, $J_{c,app} = J_{c,T}(3 - J_{c,T}/J_{c,L})/2$.
[27] Ch. Jooss, R. Warthmann, and H. Kronmüller, Phys. Rev. B **61**, 12433 (2000).
[28] Ch. Jooss, J. Albrecht, H. Kuhn, S. Leonhardt, and H. Kronmüller, Rep. Prog. Phys. **65**, 651 (2002).
[29] T. Haage, J. Q. Li, B. Leibold, M. Cardona, J. Zegenhagen, and H.-U. Habermeier, A. Forkl, Ch. Jooss, R. Warthmann, and H. Kronmüller, Solid State Commun. **99**, 553 (1996).
[30] Q. X. Jia, S. R. Foltyn, P. N. Arendt, and J. F. Smith, Appl. Phys. Lett. **80**, 1601 (2001).